Surface & Coatings Technology 364 (2019) 248–255

Contents lists available at ScienceDirect

Surface & Coatings Technology

journal homepage: www.elsevier.com/locate/surfcoat

Fabrication of porous anodic alumina (PAA) templates with straight pores and with hierarchical structures through exponential voltage decrease technique

Leandro Sacco[a,b,*], Ileana Florea[a], Costel-Sorin Cojocaru[a]

[a] LPICM, Ecole Polytechnique, CNRS, 91128 Palaiseau Cedex, France
[b] Delft University of Technology, Faculty of Electrical Engineering, Mathematics and Computer Science, Department of Microelectronics, Delft, Feldmannweg 17, 2628 CT Delft, Netherlands

ARTICLE INFO

Keywords:
Porous anodic alumina
Barrier thinning layer
Oxide barrier layer
Electrodeposition
Branches
Hierarchical nanostructures

ABSTRACT

The present work aims to become a standard step for the fabrication of the next generation porous anodic alumina (PAA) templates based devices and to provide new insights on the mechanism involved in the porous anodic alumina formation. The oxide barrier layer at the bottom of the pores has been successfully thinned by applying an exponential voltage decrease process followed by a wet chemical etching. The impact of the potential drop on the PAA structure has been deeply investigated, as well as the electrolyte temperature, the number of potential steps and the exponential decay rate. The presented results underline that a smart adjustment between the anodization conditions and exponential voltage decay parameters can simultaneously give PAA structures with straight pores and remove the dielectric layer in spite of applying the exponential voltage decay step. Additionally, the PAA structure has been tuned to fabricate hierarchically nanoporous templates with secondary pores ranging from 2 up to 10 branches.

1. Introduction

Porous anodic alumina (PAA) has attracted considerable interest as a template for the nanostructures growth [1–7]. Such template enables fabricating self-ordered hexagonal lattice with tunable geometric features by accurately adjusting the parameters involved in the anodization process. For instance, one can synthesize PAA templates with pore diameters ranging from 10 nm up to 500 nm [8–10], also with high pore densities in the range 10^8–10^{11} cm^{-2} and with pore depths from a few hundred nanometers to the millimeter scale [11]. Regarding the synthesis of nanostructures where electrodeposition processes are involved, a critical structural parameter remains the thickness of the oxide barrier layer at the pore's bottom. For example, when a thick barrier layer is perceived a high potential is required for the electrons to tunnel through such an insulating layer. Different methods have been developed in order to reduce this oxide barrier layer at the bottom of the pores. For instance, aluminum can be evaporated into a conductive substrate and subsequently the pore formation is carried out until the underlying conductive support is reached [12,13]. Nonetheless, the biggest constraint of this approach relies on the fact that an important thickness of aluminum has to be deposited since the two-step anodization process implies the elimination of a thick sacrificial layer, otherwise, a low pore ordering degree is achieved. Another approach uses free-standing membranes fabricated by the complete removal of the underlying aluminum followed by evaporation [14] or sputtered step [15] of a conductive material. However, this second approach requires two extra steps: based on deposition of a thin metal layer followed by the transfer of the alumina membrane. However, the thickness of the PAA template is limited, since the PAA membranes have to be relatively thick in order to avoid cracks. Both mentioned processes are not desirable for the high scale devices fabrication. Dry etching can be considered as a possible alternative route for removing the oxide barrier layer [16,17]. Nevertheless, this technique involves complexes and costly technologies. A straightforward procedure consists in decreasing the exponential voltage at the end of the second anodization process [18–21] followed by a wet chemical etching. The main disadvantage related to the exponential voltage decrease process is the formation of a branched structure at the bottom of the pores. The nanostructure's synthesis within a branched PAA structure has already been addressed and well reported in the literature [20,22–26]. In all these cases, the voltage decrease is implemented to generate branched nano-scale architectures. On the other hand, very interesting efforts have been

* Corresponding author at: LPICM, Ecole Polytechnique, CNRS, 91128 Palaiseau Cedex, France.
E-mail address: l.n.sacco@tudelft.nl (L. Sacco).

https://doi.org/10.1016/j.surfcoat.2019.02.086
Received 21 December 2018; Received in revised form 25 February 2019; Accepted 26 February 2019
Available online 01 March 2019
0257-8972/

devoted to fabricated straight pores applying a barrier thinning layer process, however, the adopted techniques lead to considerable pore deformation involving narrowing effects [27], or on the contrary, a pore widening phenomenon [28].

The oxide barrier is determined by the anodization conditions and is generally accepted that its thickness is proportional to the applied potential. For instance, the anodization ratio (*AR*) express the dependence between the barrier layer thickness and the applied potential, defined as $AR = t_b/U$ where t_b is the oxide barrier layer thickness and U is the anodization potential [10]. There is a huge controversy concerning the role of the electrolyte temperature on the oxide barrier thickness. Some groups report that an increasing electrolyte temperature leads to a reduction of the barrier layer thickness [29,30], on the other hand, there are studies which sustain that the barrier layer thickness is independent of the electrolyte temperature, being determined only by the applied potential [31,32]. A very interesting approach is proposed by Aerts et al. [33] who compared the influence of the aluminum temperature and the electrolyte temperature on the anodization process. They conclude that the porous oxide layer displays a larger susceptibility to the electrode temperature than to the electrolyte temperature.

In this context, the main benefit of the conducted work is to highlight that the exponential voltage decrease process can be successfully implemented to thin the oxide barrier layer at the bottom of the PAA pores avoiding a branch multiplication phenomenon, or controlling the barrier thinning parameters to precisely tailor the number of branches of the hierarchically nanotemplates. The strategy adopted for reducing the branched structure relies on a combination of a relatively high electrolyte temperature with a fast voltage drop. At every potential fall, the system enters into a new equilibrium state with a correlated pore cell structure which depends on the anodization parameters. A drastic change of the applied potential can stop the anodization process because the system cannot be self-adjusted into the newly imposed anodization conditions. Therefore, the higher electrolyte temperature implies higher density currents, consequently, for every potential drop, the system has more margins to self-adjust.

In order to estimate the number of branched, we utilize the method previously introduced [34], where we considered electrodeposited nanoparticles (NPs) which reflect the fingerprint of the previous shape/state of the bottom of the pores in order to extrapolate the number of created branched by primary pore (NBPP). To accomplish the desirable PAA structure, the impact of different synthesis parameters such as the electrolyte temperature, the voltage decay rate and the number of potential drops onto the PAA structure and the NP electrodeposited was taken into account. Focus is set on the use of the focused ion beam (FIB) technique [35,36] combined with advanced 2D TEM based techniques implemented in both the TEM and STEM imaging modes of an transmission electron microscope [37,38] to get more insight about the PAA porous structure characteristics in a nanometer range, but also to determine the precise thickness of the barrier layer at the bottom pores. Such studies set the basis to build a direct relationship between the PAA architecture in terms of pores morphology, depending on the anodization conditions, and simultaneously provide valuable information for the template fabrication.

2. Experimental

2.1. Synthesis of the PAA template

Commercial high purity aluminum foil (Alfa Aesar 99.99%, Puratronics, 0.25 mm) have been cut into 1 cm × 1 cm small pieces, cleaned in acetone and isopropanol both in an ultra-sonic bath for 15 min and subsequently rinsed with deionized water. Then, the aluminum substrates have been electropolished at 5 °C and 20 V during 6 min in a 1:4 $HClO_4$:C_2H_5OH mixture solution. PAA templates have been fabricated by a two-step anodization process in a two-electrode electrochemical cell system, Fig. 1 shows the experimental set-up

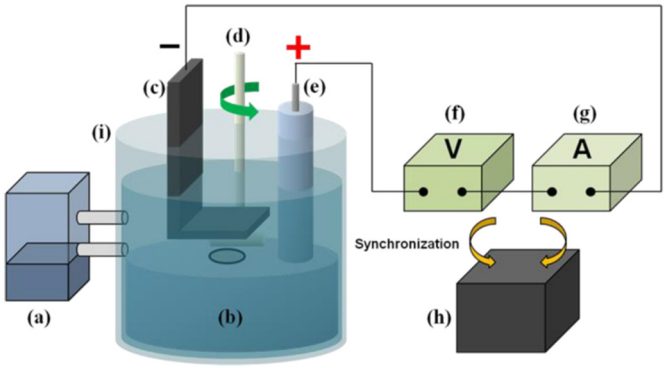

Fig. 1. Schematic diagram of the experimental set-up used for the anodization process. (a) Thermoregulator, (b) sample holder used to exposed just one side of the aluminum foil, (c) Graphite electrode, (d) motor-controlled rotator for stirring solution, (e) electrode, (f) power supply, (g) multimeter to measure current, (h) computer to operate the potentiostat, (i) thermal controlling beaker with flowing oil and the beaker for putting solution and sample holder.

implemented to carry out the anodization processes. Graphite electrode has been used as a cathode and the polished aluminum foils as an anode. The first anodization has been performed during 2 h using as electrolyte a 0.3 M oxalic acid solution at various temperatures under vigorous mechanical stirring. Previous works verify that both the temperature and the electrolyte concentration have a substantial effect on the regularity of the pore arrays [16,39], and the concentrations of impurities into the pore walls [39,40]. To obtain regular pore arrangements, only a given electrolyte concentration range matches with a specific anodization potential. Concentrations ranging from 0.3 M to 0.6 M are used for the fabrication of nanopores arrays, with a high pore order degree, anodized at 40 V in oxalic acid solutions. Lower concentrations lead to no order array of holes [41], and "burning" phenomenon takes place for higher potentials due to the Joule heating during anodization [39,42]. In the present work 0.3 M oxalic acid solution has been used because a good pore order degree can be achieved at room temperatures anodization processes. The presence of a contaminant is less relevant for the purpose of this work. However, it is important to point out that anions incorporated into the pore walls induce a decreased etching rate of PAA in the phosphoric acid, such structural parameter is of paramount importance when the oxide barrier layer has to be reduced. Nevertheless, in the present work, even if wet etching is applied to reduce the alumina layer, the most important component of the thinning process in this work relies on the potential drop decrease. This approach consists of a relatively fast change on the potential drop during the voltage decrease process preserving the ongoing anodization process, which is possible only at high current densities. Therefore, the preservation of the anodization process was adjusted controlling the electrolyte temperature at a fixed concentration (similar approach can be adopted varying both: the electrolyte temperature and concentration between 0.3 M up to 0.6 M of oxalic acid). Thus, high concentrations of oxalates incorporated into the pore walls are expected for PAA anodized for high anodization temperatures due to their associated high current densities.

The resulting PAA layer has been removed in a mixture solution 0.2 M CrO_3 and 0.6 M H_3PO_4 at 60 °C during 2 h in order to create nanoimprints with close-packed hexagonal arrays on the aluminum surface. The second anodization process has been achieved by applying the same conditions than for the first step, with anodization duration of 8 min. Immediately an exponential voltage decay process has been applied in order to thin the oxide barrier layer, as previously reported [19], the potential as a function of time $U(t)$ is expressed in the following equation:

$$U(t) = V_0 exp^{(-\eta * t)} + V' \quad (1)$$

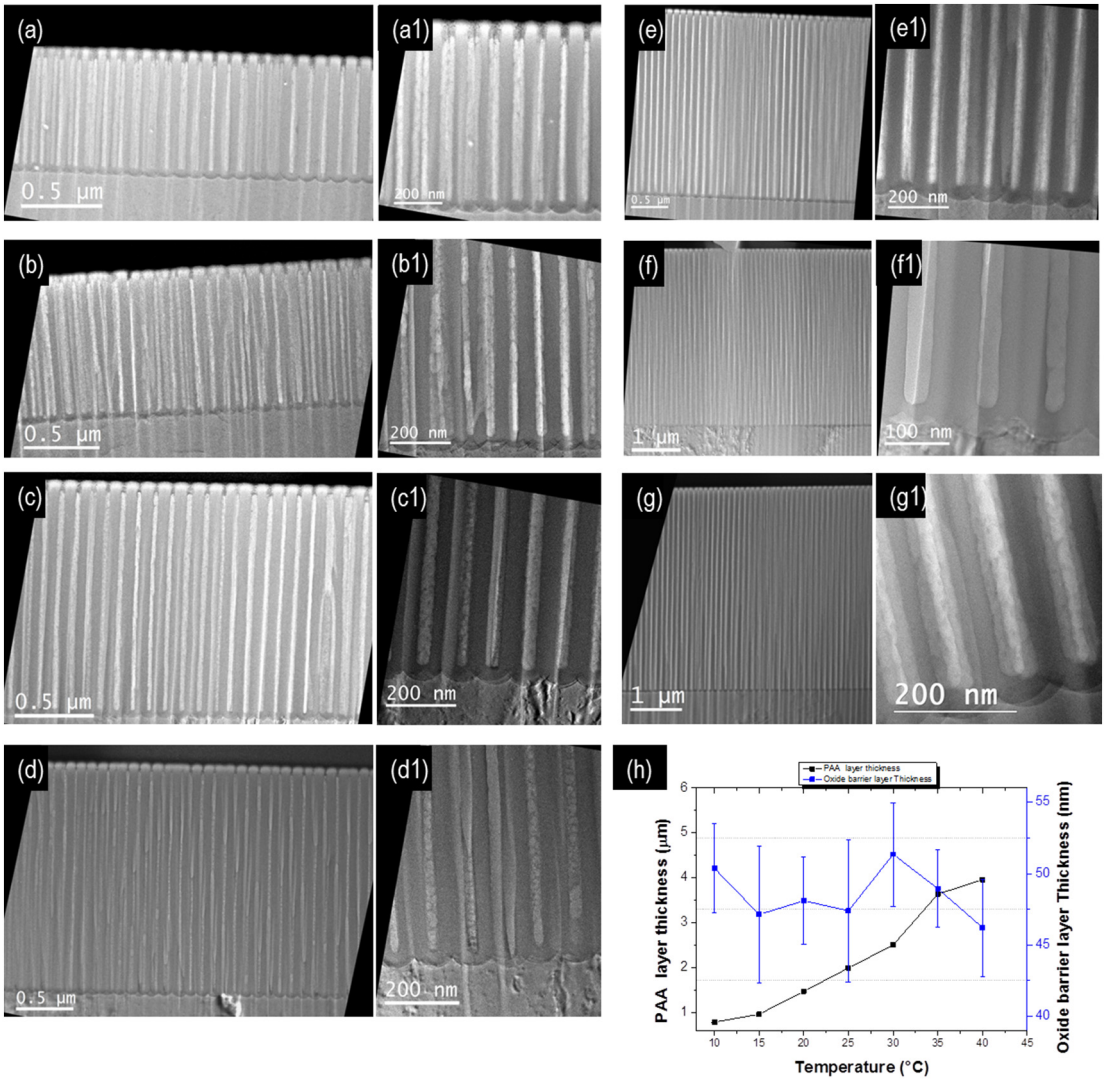

Fig. 2. Representative TEM micrographs of the PAA template synthesized for different electrolyte temperatures: 10 °C (a), 15 °C(b), 20 °C (c), 25 °C(d), 30 °C(e), 35 °C(f), 40 °C (g) evidencing the PAA pores length evolution as a function of electrolyte temperature. Figure (a1), (b1), (c1), (d1), (e1), (f1), (g1) show a zoom on the bottom part of the PAA pore evidencing the presence of the 50 nm thick barrier oxide layer; (h) Graph illustrating the evolution of the PAA and oxide barrier layer thicknesses as a function of the anodization temperature (the error value of the PAA thickness is of the order of 5%).

In the equation, the time constant η gives the rate of the voltage decrease. Different η associated at electrolyte temperatures have been used in order to study the branched multiplication phenomenon. Such parameters are summarized in Table T1 in the supplementary information (SI). The V_0 and V' are free parameters whose ideal values depend on the selected constant voltage of the PAA fabrication procedure. Herein, as previous works [19,34], for anodization step V_0 and V' have been set at 50 V and −10 V respectively. The final anodization potential applied has been set at 4.97 V. Three different numbers of total voltage drops have been applied: 394, 197 and 98. A Keithley 4200 power supply has been used for the anodization and the exponential voltage decrease processes. In order to fully remove the oxide barrier layer at the bottom of the pores, the resulting PAA templates have been immersed in a wet chemical etching solution 0.3 M H_3PO_4 at 30 °C during 25 min.

2.2. Catalyst electrodeposition

Nickel (Ni) nanoparticles (NPs) have been deposited within the PAA template using a three-electrode configuration with an Ag/AgCl electrode used as a reference electrode (RE), the PAA template used as a working electrode (WE) and a graphite electrode which acts as a counter electrode (CE). The setup was supplied through a Bio-Logic potentiostat. In order to set the electrodeposition parameters the EC-lab software has been employed. This software allows designing the shape of the pulsed applied to the working electrode. The electrodeposition process has been performed in a Watts bath solution consisting of a mixture of 330 g/L $NiO_4{\cdot}6H_2O$, 45 g/L $NiCl_2{\cdot}6H_2O$, and 45 g/L H_3BO_3. For our deposition experiment, we chose to use the pulsed mode during which the deposition step is alternated by applying a −5.5 V potential for 5 ms between the WE and the RE, followed by 90 ms resting time in the open voltage circuit mode. For the fabrication of the entire sets of samples, the number of total sweeps has been set at 50, the Watts bath temperature has been kept at 20 °C for all the deposition processes.

2.3. Characterization techniques

The morphological characterizations have been performed using a Field-Emission Scanning Electronic Microscopy (FE-SEM, HITACHI S4800). As in our previous work [43], the main pore characteristics of the PAA templates, such as the pore area, the pore diameter and their boundary have been measured directly from the SEM micrographs

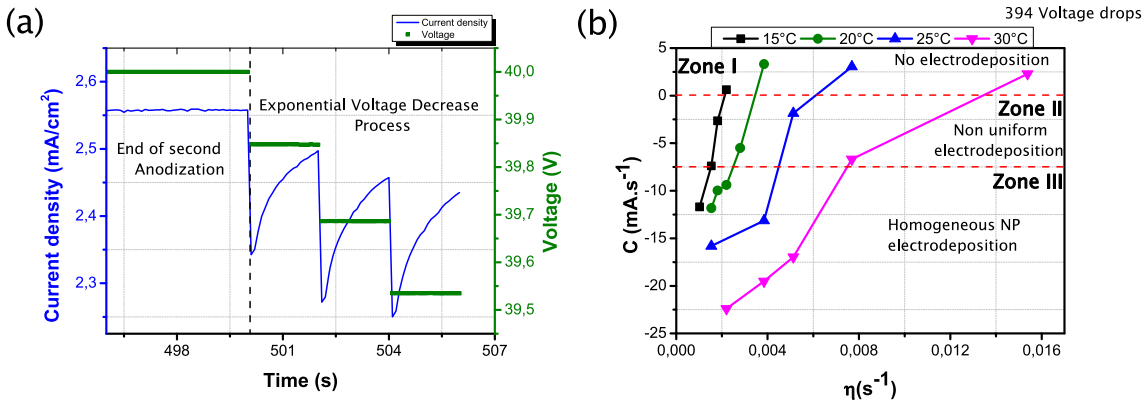

Fig. 3. The two criteria considered for determining the corresponding values of the exponential voltage decays rate (η) which lead to an effective barrier thinning process. (a) Applied voltage (represented in green) and anodization current (represented in blue) curves as a function of time at the end of the second anodization process and at the beginning of the exponential voltage decrease. After every voltage drop the anodization current (blue) increase until the next voltage fall. (b) The relation between the global charges accumulated during the electrodeposition process into PAA templates fabricated at different temperatures as a function of η. Only the zone where a uniform NP distribution is obtained provides effectives η values for the thinning process. (For interpretation of the references to colour in this figure legend, the reader is referred to the web version of this article.)

using image treatment through the open-source "ImageJ" software [44]. For a more detailed description of the PAA, features see the SI. For the TEM analyses of all the synthesized samples, cross-section lamella preparation was necessary [45]. Such preparation has been performed within a Scios DualBeam instrument a combination of a Scanning Electron microscope (SEM) operating at 30 kV that produce enlarged images of the studied materials and a Focused Ion Beam (FIB) system containing a Gallium (Ga) source capable of fast and precise milling of the materials. For the cross-section lamella preparation high Ga beam energy has been used in a first step in order to isolate an area of interest within the sample and stick it to the TEM grid substrate. Then in order to reduce the Ga implantation within the sample and the damage produced by the Ga impact during preparation, we reduced the Ga beam energy from 30 kV to 2 kV during the thinning process. The transmission electron microscopy (TEM) observations were carried out using two FEI-Titan G2 transmission electron microscopes operating at 200 kV and 300 kV. The TEM operating at 300 kV was used for accessing the morphological characteristics of each prepared sample. The TEM operating at 200 kV equipped with a Cs probe corrector and a Chemistem Super-X detector allowed us achieving chemical analyses using Energy Dispersive X-ray spectroscopy (EDX). The chemical analyses were performed using the scanning transmission imaging mode (STEM) of the microscope which consist in using a convergent electron probe to scan the sample and collecting the electrons scattered at high angle. Thus, the signal recorded in this mode is proportional to the atomic number Z of the probed sample providing information on the chemical composition of the analyzed sample, an incoherent imaging mode, called High-Angle Annular Dark Field (HAADF).

3. Results and discussion

3.1. PAA dependence with the anodization temperature

In order to study the pore's bottom zone, PAA templates have been fabricated by considering different electrolyte temperatures (without applying a thinning barrier step process). The TEM micrographs obtained for each corresponding PAA templates given in Fig. 2(a)–(g), evidence the effect of the electrolyte temperature on the PAA template characteristics in terms of pores length and structure. In Fig. S1 is well evidenced that the current density is affected by the electrolyte temperature. It is well known that the electrolyte solution and the solid electrode are characterized by different types of conductivity: electron current passes through aluminum, and ionic current through the electrolyte solution. For the current to pass through the interface between them, the following electrochemical reaction must occur: $Al + 2H_2O \rightarrow Al(O)OH + 3H+ + 3e^-$. In this reaction, protons are generated along with the electrons for the external circuit, which decreases the pH value at pore bottoms and promotes the in-situ dissolution of alumina leading to a rise of the anodization current [46], the ion current is driving force for oxide growth, while electronic current results in oxygen evolution under the contaminated anion layer [47]. Consequently, the increment of current densities driven by higher electrolyte temperatures, leads to a pore length variation from 0.9 µm up to 5 µm, in the range of anodization temperatures from 10 °C to 40 °C, as shows Fig. 2h. This set of experiments also shed light on the dependence of the oxide barrier thickness as a function of the anodization temperature. Independently of the electrolyte temperature, the dielectric layer thickness remains 50 nm. Particularly, for the whole range of electrolyte temperature, herein $AR = (1.20 \pm 0.05)$ nm/V which is in perfect agreement with previous works [4]. The results obtained allow us to sustain that the electrolyte temperature doesn't entail any structural advantage to thin the dielectric barrier thickness.

Detailed explanation concerning the effect of the electrolyte temperature on the PAA structure is shown in the supporting information material (Figs. S1 and S2). Pore characteristics such as pore diameter, interpore distance, porosity, pore density, circularity, and pore regularity are calculated as in our previous publication [43].

3.2. Exponential voltage decrease

The branch multiplication is a phenomenon consequence of the exponential voltage decrease, especially when a potential step is kept for a long period. This phenomenon has been even applied [48] to fabricated branched pores and then form Y-branched nanowires. In the present work, various voltage decays rate have been used with an associated electrolyte temperature. However, it's very complicated and time-consuming to establish by direct measurements, i.e. FIB manipulation and TEM observations [49], if the exponential voltage decays rate η is effective to thin the oxide barrier layer. The situation is aggravated when a branched structure is present at the bottom of the pores. Therefore, to determine an effective η value, we have taken into account two criteria. The first one refers to the fact that the anodization voltage is not interrupted during the whole exponential voltage decrease process. This implies an increase of the current density followed the voltage drop as is pointed out in Fig. 3(a). Such rise of the current density guaranteed the ongoing anodization process, since the system is self-adjusted to new a cell structure associated with a steady density current, nevertheless, herein the potential drops before the system

reaches a steady state [18]. The second criterion, consider that a homogenous electrodeposition process occurs subsequently to the thinning process. In order to verify this assumption nickel nanoparticles have been deposited within the PAA template at various η. Fig. 3(b) summarizes the cumulated charged during the electrodeposition process for four different electrolyte temperatures (15 °C, 20 °C, 25 °C and 30 °C). As it can be depicted three zones in the plot are delimited as a function of the homogeneity of the electrodeposition process, Fig. S4 in SI summarize typical NP distribution for each zone. Taking into account that for Ni nanoparticles electrodeposition, a redox reaction takes place, the total accumulated charge during the whole process has to be negative. Cumulated charge (C) values close to zero indicates that the thickness oxide barrier layer imposed a barrier potential that hinders the electrodeposition process, consequently, there are not NP deposited (Zone I). When the thinning process is effective only in certain spots, electrodeposition process takes place preferentially in such zones, leading to a non-homogeneous NP distribution, as is pointed out in Fig. S2(b), under the presented fabrication condition such kind of NP distributions are obtained for C values ranging from -5 mA·s to -1 mA·s (Zone II). In case of a uniform thinning oxide barrier thickness, the electrodeposition process takes places in each pore leading to uniform distribution of individual electrodeposited NP, the associated C values which correspond with these kind of NP distributions ranged from -22 mA·s up to -10 mA·s (Zone III). Therefore, Fig. 3(b) provides valuable information of which exponential decay rate (η) associated with which anodization temperature should be selected to effectively reduce the oxide barrier layer at the bottom of the pores, enabling the study of the branch multiplication phenomenon generated by the exponential voltage decrease process.

As stated before, for many nanotechnological applications, is of paramount importance to control the number of branches or to execute the thinning barrier process avoiding a branch generation. In order to address this problem, we calculated the Number of Branches generated by Primary Pore (NBPP) as a function of the exponential voltage, applying three different total number of voltage drops. Fig. 4(a) summarizes the estimated NBPP as a function of the exponential voltage decay rate for PAA templates fabricated at different anodization temperatures by considering three different number of voltage steps (98 steps – filled triangle, 197 steps – filled circle and 398 steps-filled square). For each exponential decay and number of potential drops, only a range of electrolyte temperature is compatible with a thinning barrier process. On one hand, high anodization temperatures lead to high current densities, increasing the rate of O_2 produced during the anodization, triggering to an abundant gas production that can hinder the ion diffusion that will disrupt the self-ordering process [45]. On the other hand, too low electrolyte temperatures cannot follow the anodization process during the exponential voltage decay process. Therefore, the anodization temperature was set as the minimum electrolyte temperature that simultaneously guaranteed both criteria summarized in Fig. 3 (ongoing anodization process and uniform electrodeposition).

PAA templates with straight pores are pointed out in the Fig. 4(a) by green triangles corresponding to a temperature of 32.5 °C, 98 steps and an exponential voltage decay of $2.28 \times 10^{-3}\,s^{-1}$. Fig. 4(b) contains a SEM micrograph illustrating the Ni NP distribution after the removal of the PAA template by a chemical etching described elsewhere [43]. The yellow circles in the micrograph point out two honeycomb patterns representative of PAA templates. In inset, the SEM image of the PAA template before the PAA removal evidencing the presence of its honeycomb pattern.

In order to verify simultaneously the consistency of our method based on the comparison between the number of NP and the pore densities, with the fact that straight pores can be fabricated although an exponential voltage decrease process is considered, STEM-EDX analyses have been performed. This type of analyses enables accessing direct information regarding, both the PAA pore length and the Ni NPs characteristics, such as their size and exact localization. In the STEM-

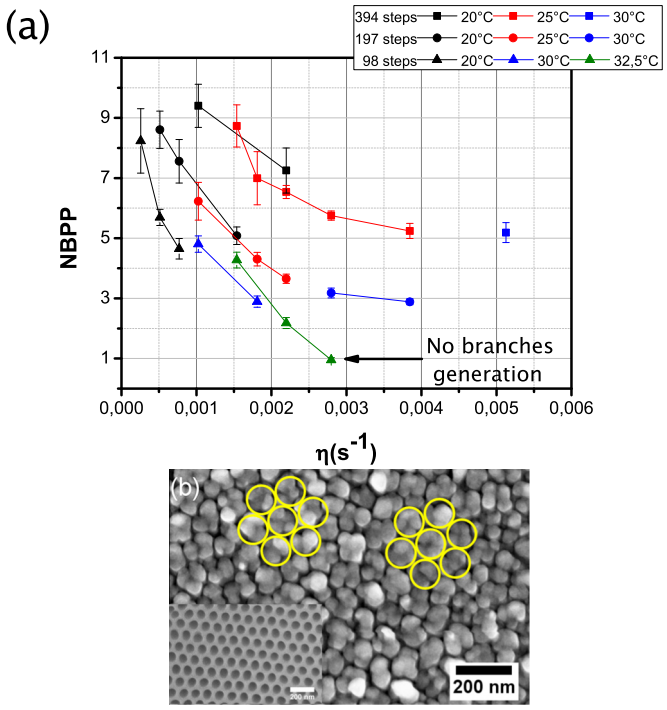

Fig. 4. (a) Number of Branches generated by Primary Pore (NBPP) as a function of the exponential voltage decay rate at different anodization temperatures and various number of voltage steps. (b) SEM micrograph evidencing the Ni NPs deposition after the PAA removal via a chemical etching. The PAA template has been prepared using the condition for which no branch formation is expected. The anodization temperature was set at 32.5 °C, the total number of steps was 98 and the exponential voltage decay was $2.28 \times 10^{-3}\,s^{-1}$. In yellow is pointed out the former pores positions. (For interpretation of the references to colour in this figure legend, the reader is referred to the web version of this article.)

HAADF micrograph represented in Fig. 5(a) are shown the straight pores along the PAA layer with the Ni NPs deposited at the bottom of the pores. The corresponding STEM-HAADF-EDX relative map is given in Fig. 5(b), obtained by considering as element of interests: aluminum (Kα = 1.46 eV), oxygen (Kα = 0.5 23 eV), and nickel (Kα = 7.4 77 eV). The relative map reveals the presence of the Ni NPs within the PAA porous structure. A closer analysis on the Ni NP present inside the pores, see the inset in Fig. 5(b), evidences the presence of a 5 nm oxygen layer at the bottom part of the Ni nanoparticle, characteristic of the native oxide barrier layer of the aluminum. These findings highlight that the applied procedure successfully reduces the thickness of the oxide dielectric barrier of the PAA templates. For the very first time are shown straight pores after the application of an exponential voltage decrease process.

Fig. 4(a) provides valuable information for the fabrication of nanoporous templates with straight pores and hierarchical structures with up to 10 branches created by the primary pore. The number of total voltage steps has a great impact on the pore bottom structure. As described above, in steady anodization, the thickness of the dielectric barrier t_B is proportional to the applied potential. However in the case of the exponential voltage decrease where a non-steady process takes place the barrier thickness depend on the anodized potential given by the Eq. (1), where is parameterized by η. Since the effectiveness of the exponential voltage decrease process is affected by the electrolyte temperature T_e, the oxide barrier layer also strongly depend of the electrolyte temperature. Therefore for the non-steady anodization processes, we can establish that $t_B = t_B(U,\eta,T_e)$. On the other hand, we infer that the number of voltage steps determines the NBPP. For instance, higher branches densities are obtained for PAA templates

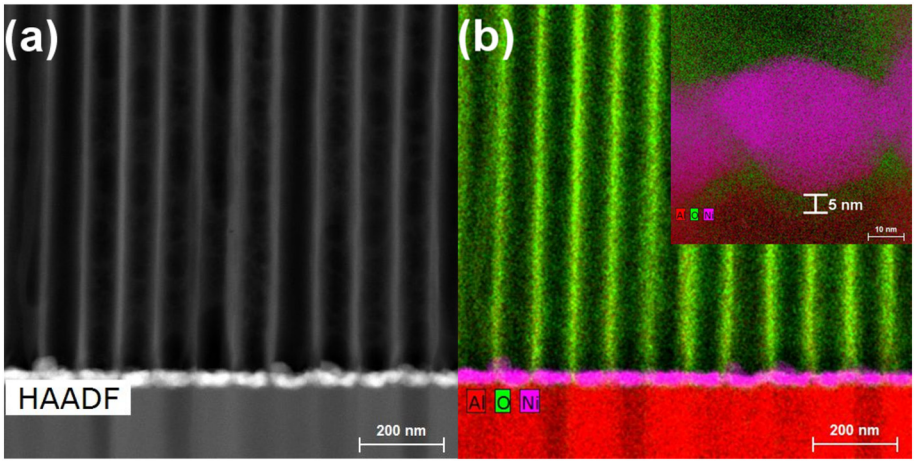

Fig. 5. (a) STEM HAADF micrograph of a FIB cross-section lamella of Ni NP within the PAA template fabricated using the condition for which no branch formation is expected. (b) The corresponding STEM-EDX relative map with the aluminum represented in red, oxygen in green and nickel in pink; in inset, high-resolution STEM-EDX relative map on the Ni NP at the bottom part of the PAA pores evidencing the presence of 5 nm oxide barrier layer left after the thinning procedure. (For interpretation of the references to colour in this figure legend, the reader is referred to the web version of this article.)

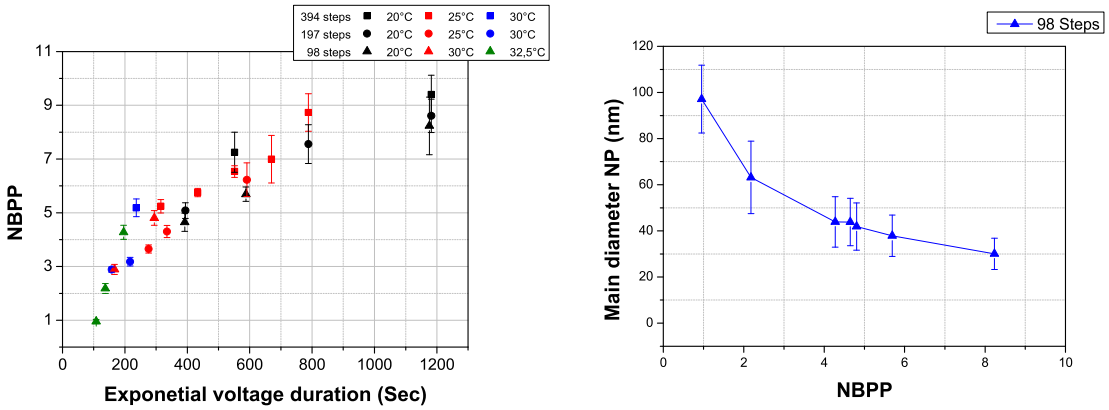

Fig. 6. Influence of the exponential voltage duration. (a) NBPP as a function of the exponential voltage duration at different anodization temperatures and various number of voltage steps. (b) Nanoparticles diameter as a function of NBPP.

fabricate with the same η value but with a higher number of voltage drops. This is consistent with the fact that more potentials drops entails longer voltage decrease process, consequently, the system has more time to create branches. Fig. 6 summarizes the effects of the exponential voltage duration. Fig. 6(a) plots the NBPP as a function of the exponential voltage decrease duration. Such graph reflects the fact that the number of branches is approximately the same for PAA fabricated with different η and number of total steps, but with the same anodization time. In addition, such plot evidenced that higher exponential voltage decrease durations lead to an increment of the branch multiplication phenomenon which implies a higher pore density. Then the sizes of each secondary created branch have a smaller size for a longer anodization process. Fig. 6(b) shows the NP size as a function of the NBBP, as expected, when no branches are created the pore size and the NP size matches. As more branches are created the pores reduced their size.

3.3. Straight pore formation

The previous results reveal that the anodization temperature and the exponential voltage decay rate mainly determine the pore structure close to oxide/aluminum interphase. In order to get a deeper understanding of the branched multiplication is interesting to roughly estimate the density of pores during the exponential decay process and the influence of the anodization temperature on the PAA geometrical features.

The pore density (n) and porosity (α) at the fixed potential for a hexagonal close packed array is given respectively by Eqs. (2) and (3) [50].

$$n = \frac{\alpha}{\pi}\left(\frac{2}{D_P}\right)^2 10^{14} \tag{2}$$

$$\alpha = \frac{\pi}{2\sqrt{3}}\left(\frac{D_P}{D_I}\right)^2 \tag{3}$$

where D_I and D_P are the interpore distance and the pore diameter, is generally accepted that D_P and D_I can be expressed as a function of the anodization potentials. In particular D_I can be expressed as in Eq. (4) where λ_I is proportionality a constant [51].

$$D_I = \lambda_I * U_{Anod} \tag{4}$$

Then, the density of pores defined as a total number of pores in square of 1 cm^2 is given by:

$$n = \frac{1}{{D_I}^2}\left(\frac{2}{\sqrt{3}}\right) \times 10^{14} \tag{5}$$

Manipulating these set of equations with (1), is possible to infer a temporal evolution of the amount of branches, comparing the pore density at time $n(t)$ with the initial pore density, $n(t = 0)$, as express Eq. (6),

$$\frac{n(t)}{n(t=0)} = \left(\frac{V_0 + V'}{V_0 exp^{(-\eta * t)} + V'}\right)^2 \tag{6}$$

It is important to highlight that such relation loses its validity as the anodized PAA layers start to differ from hexagonal patterns, therefore we cannot exactly calculate the NBBP for the PAA fabricated in our work, since the final applied potential is 4. 97 V, which highly differs from ideally optimal anodization potential in oxalic acidic environment

which corresponds to 40 V [52]. Notice all the formalism applied within Eqs. (2) and (6) relies on branches obtained in steady-state conditions. Therefore, only conclusions concerning the trend of the number of branches can be inferred, such as fact that fasters exponential decrease processes reduce the number of branches. More efforts should be performed to describe the pore morphologies in the non-steady anodization regime since branches formed under non-steady conditions are not predictable based on the currently available models.

However, in order to explain the formation of straights pores, we propose a pore formation mechanism which considers that the branched pores are still formed after each potential drops, but for fast voltages decay rates which effectively reduced the oxide layer, the small pore branches are dissolved due to a pore merging triggered by the high electrolyte temperature that etches the pores walls. Such idea is in harmony with the fact that the pore diameter considerably increases as the electrolyte temperature rise, while the interpore distance does not significantly vary as a function of the electrolyte temperature (see Fig. S3). Nevertheless, to achieve this PAA formation condition, a fine tune of η is required, as evidence Fig. 4(a), an increment of the decay rate lead to a branch multiplication phenomenon.

4. Conclusions

In summary, herein we developed a powerful procedure that enables to homogeneously remove the oxide barrier layer at the bottom of the pores which limits and complicates the synthesis of nanostructures for the development of further applications. For the first time, we directly showed the possibility to implement the exponential voltage decrease process without the creation of secondary pores. The results obtained on the described methodology clearly show that by accurately adjusting the parameters involved in the anodization process, it is possible to fabricate nanotemplates with straight pores either hierarchically structures with up to 10 branches created per primary pore. We corroborate that in the steady anodization process the oxide barrier layer is only determined by the applied potential. However, the electrolyte temperature in the exponential voltage decrease process plays a key role since enables to increase the anodization current. Thus, faster voltage drops can be applied without interrupting the pore formation and consequently enlarging the range of η effective to thin the dielectric barrier layer. The number of branches created by primary pore (NBPP) is mainly determinate by such effective's η values, and the exponential voltage duration. Shorter thinning processes duration lead to a reduction of branch multiplication phenomenon, straight pores can be fabricated when interpore walls are dissolved and the small branched pores are merged due to high electrolyte temperature that wider the pore diameter. The methodology introduced can be rapidly converted as a building block for the next generation of devices based on PAA templates.

Acknowledgements

L. S. gratefully acknowledges financial support from the Chaire de Recherche PSA AC3M sponsored by Citroën at the Ecole Polytechnique and Chaire EXXI sponsored by EDF at Ecole Polytechnique. The authors acknowledge financial support from the French state managed by the French National Research Agency under the Investments for the Future program under the reference ANR-10-EQPX-50, pole Tempos-NanoTEM and pole TEMPOS NanoMax.

Appendix A. Supplementary data

Supplementary data to this article can be found online at https://doi.org/10.1016/j.surfcoat.2019.02.086.

References

[1] Y.S. Cheng, N.F. Wang, Y.Z. Tsai, J.J. Lin, M.P. Houng, Investigation of CuInSe2nanowire arrays with core–shell structure electrodeposited at various duty cycles into anodic alumina templates, Appl. Surf. Sci. 396 (2017) 631–636, https://doi.org/10.1016/j.apsusc.2016.10.207.
[2] K.H. Kim, D. Brunel, A. Gohier, L. Sacco, M. Châtelet, C.S. Cojocaru, Cup-stacked carbon nanotube schottky diodes for photovoltaics and photodetectors, Adv. Mater. 26 (2014) 4363–4369, https://doi.org/10.1002/adma.201400775.
[3] A. Drury, S. Chaure, M. Kröll, V. Nicolosi, N. Chaure, W.J. Blau, Fabrication and characterization of silver/polyaniline composite nanowires in porous anodic alumina, Chem. Mater. 19 (2007) 4252–4258, https://doi.org/10.1021/cm071102s.
[4] W. Lee, S.-J. Park, Porous anodic aluminum oxide: anodization and templated synthesis of functional nanostructures, Chem. Rev. 114 (2014) 7487–7556, https://doi.org/10.1021/cr500002z.
[5] A. Li, S. Pan, X. Dou, Y. Zhu, X. Huang, Y. Yang, G. Li, L. Zhang, Direct electrodeposition of ZnO nanotube arrays in anodic alumina membranes, J. Phys. Chem. C 111 (2007) 7288–7291, https://doi.org/10.1021/jp0711242.
[6] J. Kim, D.H. Lee, J.H. Kim, S.H. Choi, Graphene-assisted chemical etching of silicon using anodic aluminum oxides as patterning templates, ACS Appl. Mater. Interfaces 7 (2015) 24242–24246, https://doi.org/10.1021/acsami.5b07773.
[7] H. Zhou, R. Chang, E. Reichmanis, Y. Song, Wetting of inkjet polymer droplets on porous alumina substrates, Langmuir 33 (2017) 130–137, https://doi.org/10.1021/acs.langmuir.6b03820.
[8] O. Nishinaga, T. Kikuchi, S. Natsui, R.O. Suzuki, Rapid fabrication of self-ordered porous alumina with 10-/sub-10-nm-scale nanostructures by selenic acid anodizing, Sci. Rep. 3 (2013) 2748, , https://doi.org/10.1038/srep02748.
[9] W. Lee, R. Ji, U. Gösele, K. Nielsch, Fast fabrication of long-range ordered porous alumina membranes by hard anodization, Nat. Mater. 5 (2006) 741–747, https://doi.org/10.1038/nmat1717.
[10] M. Yu, W. Zhang, S. Zhang, S. Zhao, F. Ai, X. Zhu, Morphology evolution of porous anodic alumina in mixed H3PO4/NH4F electrolytes, Surf. Coat.Technol. 334 (2018) 500–508, https://doi.org/10.1016/j.surfcoat.2017.12.012.
[11] Y. Lin, Q. Lin, X. Liu, Y. Gao, J. He, W. Wang, Z. Fan, A highly controllable electrochemical anodization process to fabricate porous anodic aluminum oxide membranes, Nanoscale Res. Lett. 10 (2015) 1–8, https://doi.org/10.1186/s11671-015-1202-y.
[12] C. Rochford, S.J. Limmer, S.W. Howell, T.E. Beechem, M.P. Siegal, Planarized arrays of aligned, untangled multiwall carbon nanotubes with Ohmic back contacts, J. Mater. Res. 30 (2014) 315–322, https://doi.org/10.1557/jmr.2014.359.
[13] D.K. Ivanou, Y.A. Ivanova, A.D. Lisenkov, M.L. Zheludkevich, E.A. Streltsov, Electrochemical deposition of lead and tellurium into barrierless nanoporous anodic aluminium oxide, Electrochim. Acta 77 (2012) 65–70, https://doi.org/10.1016/j.electacta.2012.05.061.
[14] D. Xu, Y. Xu, D. Chen, G. Guo, L. Gui, Y. Tang, Preparation and characterization of CdS nanowire arrays by dc electrodeposit in porous anodic aluminum oxide templates, Chem. Phys. Lett. 325 (2000) 340–344, https://doi.org/10.1016/S0009-2614(00)00676-X.
[15] N. Zafar, S. Shamaila, R. Sharif, H. Wali, S. Naseem, S. Riaz, M. Khaleeq-Ur-Rahman, Effects of pH on the crystallographic structure and magnetic properties of electrodeposited cobalt nanowires, J. Magn. Magn. Mater. 377 (2015) 215–219, https://doi.org/10.1016/j.jmmm.2014.10.105.
[16] L. Ba, W.S. Li, Influence of anodizing conditions on the ordered pore formation in anodic alumina, J. Phys. D. Appl. Phys. 33 (2000) 2527–2531, https://doi.org/10.1088/0022-3727/33/20/302.
[17] J. Liang, H. Chik, A. Yin, J. Xu, Two-dimensional lateral superlattices of nanostructures: nonlithographic formation by anodic membrane template, J. Appl. Phys. 91 (2002) 2544–2546, https://doi.org/10.1063/1.1433173.
[18] A.P. Furneax, R.C. Rigby, W.R. Davidson, The formation of controlled-porosity membranes from andically oxidized aluminum, Nature. 337 (1989) 147, https://doi.org/10.1038/337147a0.
[19] B. Marquardt, L. Eude, M. Gowtham, G. Cho, H.J. Jeong, M. Châtelet, C.S. Cojocaru, B.S. Kim, D. Pribat, Density control of electrodeposited Ni nanoparticles/nanowires inside porous anodic alumina templates by an exponential anodization voltage decrease, Nanotechnology. 19 (2008) 405607, , https://doi.org/10.1088/0957-4484/19/40/405607.
[20] W.J. Stepniowski, M. Moneta, K. Karczewski, M. Michalska-Domanska, T. Czujko, J.M.C. Mol, J.G. Buijnsters, Fabrication of copper nanowires via electrodeposition in anodic aluminum oxide templates formed by combined hard anodizing and electrochemical barrier layer thinning, J. Electroanal. Chem. 809 (2018) 59–66, https://doi.org/10.1016/j.jelechem.2017.12.052.
[21] P.G. Schiavi, P. Altimari, A. Rubino, F. Pagnanelli, Electrodeposition of cobalt nanowires into alumina templates generated by one-step anodization, Electrochim. Acta 259 (2018) 711–722, https://doi.org/10.1016/j.electacta.2017.11.035.
[22] C.T. Sousa, A. Apolinario, D.C. Leitao, A.M. Pereira, J. Ventura, J.P. Araujo, Precise control of the filling stages in branched nanopores, J. Mater. Chem. 22 (2012) 3110, https://doi.org/10.1039/c2jm14828e.
[23] W. Cheng, M. Steinhart, U. Gösele, R.B. Wehrspohn, Tree-like alumina nanopores generated in a non-steady-state anodization, J. Mater. Chem. 17 (2007) 3493, https://doi.org/10.1039/b709618f.
[24] G. Meng, Y.J. Jung, A. Cao, R. Vajtai, P.M. Ajayan, Controlled fabrication of hierarchically branched nanopores, nanotubes, and nanowires, Proc. Natl. Acad. Sci. U. S. A. 102 (2005) 7074–7078, https://doi.org/10.1073/pnas.0502098102.
[25] B. Chen, Q. Xu, X. Zhao, X. Zhu, M. Kong, G. Meng, Branched silicon nanotubes and metal nanowires via AAO-template-assistant approach, Adv. Funct. Mater. (2010)

3791–3796, https://doi.org/10.1002/adfm.201001190.
[26] Y.T. Kim, J. Schilling, S.L. Schweizer, R.B. Wehrspohn, High density Ag nanobranches decorated with sputtered Au nanoparticles for surface-enhanced Raman spectroscopy, Appl. Surf. Sci. 410 (2017) 525–529, https://doi.org/10.1016/j.apsusc.2017.02.167.
[27] W.J. Stępniowski, W. Florkiewicz, M. Michalska-Domańska, M. Norek, T. Czujko, A comparative study of electrochemical barrier layer thinning for anodic aluminum oxide grown on technical purity aluminum, J. Electroanal. Chem. 741 (2015) 80–86, https://doi.org/10.1016/J.JELECHEM.2015.01.025.
[28] G. Sauer, G. Brehm, S. Schneider, K. Nielsch, R.B. Wehrspohn, J. Choi, H. Hofmeister, U. Gösele, Highly ordered monocrystalline silver nanowire arrays, J. Appl. Phys. 91 (2002) 3243–3247, https://doi.org/10.1063/1.1435830.
[29] J.P. O'Sullivan, G.C. Wood, The morphology and mechanism of formation of porous anodic films on aluminium, Proc. R. Soc. A Math. Phys. Eng. Sci. 317 (1970) 511–543, https://doi.org/10.1098/rspa.1970.0129.
[30] G.D. Sulka, Highly ordered anodic porous alumina formation by self-organized anodizing, Nanostructured Mater. Electrochem, 2008, pp. 1–116, , https://doi.org/10.1002/9783527621507.ch1.
[31] A.M. Abd-Elnaiem, A. Gaber, Parametric study on the anodization of pure aluminum thin film used in fabricating nano-pores template, Int. J. Electrochem. Sci. 8 (2013) 9741–9751.
[32] C.H. Voon, M.N. Derman, U. Hashim, K.R. Ahmad, K.L. Foo, Effect of temperature of oxalic acid on the fabrication of porous anodic alumina from Al-Mn alloys, J. Nanomater. 2013 (2013), https://doi.org/10.1155/2013/167047.
[33] T. Aerts, J.B. Jorcin, I. De Graeve, H. Terryn, Comparison between the influence of applied electrode and electrolyte temperatures on porous anodizing of aluminium, Electrochim. Acta 55 (2010) 3957–3965, https://doi.org/10.1016/j.electacta.2010.02.044.
[34] L. Sacco, I. Florea, M. Châtelet, C.-S. Cojocaru, Electrical and morphological behavior of carbon nanotubes synthesized within porous anodic alumina templates, J. Phys. Mater. 1 (2018) 015004, , https://doi.org/10.1088/2515-7639/aad57f.
[35] M. Schaffer, B. Schaffer, Q. Ramasse, Sample preparation for atomic-resolution STEM at low voltages by FIB, Ultramicroscopy. 114 (2012) 62–71, https://doi.org/10.1016/j.ultramic.2012.01.005.
[36] N.D. Bassim, B.T. De Gregorio, A.L.D. Kilcoyne, K. Scott, T. Chou, S. Wirick, G. Cody, R.M. Stroud, Minimizing damage during FIB sample preparation of soft materials, J. Microsc. 245 (2012) 288–301, https://doi.org/10.1111/j.1365-2818.2011.03570.x.
[37] I. Florea, C. Feral-Martin, J. Majimel, D. Ihiawakrim, C. Hirlimann, O. Ersen, Three-dimensional tomographic analyses of ceo2nanoparticles, Cryst. Growth Des. 13 (2013) 1110–1121, https://doi.org/10.1021/cg301445h.
[38] O. Ersen, I. Florea, C. Hirlimann, C. Pham-Huu, Exploring nanomaterials with 3D electron microscopy, Mater. Today 18 (2015) 395–408, https://doi.org/10.1016/j.mattod.2015.04.004.
[39] C.K. Chung, D. Dhandapani, C.J. Syu, M.W. Liao, B.Y. Chu, E.H. Kuo, Role of oxalate anions on the evolution of widened pore diameter and characteristics of room-temperature anodic aluminum oxide, J. Electrochem. Soc. 164 (2017) C121–C127.
[40] K.S. Choudhari, S.D. Kulkarni, S.C., S.D. George, Influence of Electrolyte Composition on the Photoluminescence and Pore Arrangement of Nanoporous Anodic Alumina, ECS J. Solid State Sci. Technol. 7 (2018) R175–R182. doi:https://doi.org/10.1149/2.0081811jss.
[41] M.A. Kashi, A. Ramazani, The effect of temperature and concentration on the self-organized pore formation in anodic alumina, J. Phys. D. Appl. Phys. 38 (2005) 2396–2399, https://doi.org/10.1088/0022-3727/38/14/015.
[42] N.-Q. Zhao, X.-X. Jiang, C.-S. Shi, J.-J. Li, Z.-G. Zhao, X.-W. Du, Effects of anodizing conditions on anodic alumina structure, J. Mater. Sci. 42 (2007) 3878–3882.
[43] L. Sacco, I. Florea, M. Châtelet, C.-S. Cojocaru, Investigation of porous anodic alumina templates formed by anodization of single-crystal aluminum substrates, Thin Solid Films 660 (2018) 213–220, https://doi.org/10.1016/J.TSF.2018.06.015.
[44] C.A. Schneider, W.S. Rasband, K.W. Eliceiri, NIH image to ImageJ: 25 years of image analysis, Nat. Methods 9 (2012) 671–675, https://doi.org/10.1038/nmeth.2089.
[45] I. Florea, L.N. Sacco, M. Chatelet, C. Cojocaru, 2D-TEM investigations of CNT s synthetized within vertical-PAA templates for devices applications, in: Eur. Microsc. Congr. 2016 Proc., Wiley Online Library, 2016: pp. 922–923.
[46] B. Chong, D. Yu, R. Jin, Y. Wang, D. Li, Y. Song, M. Gao, X. Zhu, Theoretical derivation of anodizing current and comparison between fitted curves and measured curves under different conditions, Nanotechnology. 26 (2015) 145603, , https://doi.org/10.1088/0957-4484/26/14/145603.
[47] Y. Zhang, W. Cheng, F. Du, S. Zhang, W. Ma, D. Li, Y. Song, X. Zhu, Quantitative relationship between nanotube length and anodizing current during constant current anodization, Electrochim. Acta 180 (2015) 147–154, https://doi.org/10.1016/J.ELECTACTA.2015.08.098.
[48] L. Zaraska, E. Kurowska, G.D. Sulka, M. Jaskuła, Porous alumina membranes with branched nanopores as templates for fabrication of Y-shaped nanowire arrays, J. Solid State Electrochem. 16 (2012) 3611–3619, https://doi.org/10.1007/s10008-012-1795-3.
[49] S. Lee, D. Kim, E. Gillette, J. Oh, S.W. Han, S.B. Lee, Anodized pore structural evolution of focused ion beam patterned Al: direct analysis of branched nanopores and nanosacks, Phys. Chem. Chem. Phys. 15 (2013) 10659, , https://doi.org/10.1039/c3cp50630d.
[50] M. Michalska-Domańska, W.J. Stępniowski, L.R. Jaroszewicz, Characterization of nanopores arrangement of anodic alumina layers synthesized on low-(AA1050) and high-purity aluminum by two-step anodizing in sulfuric acid with addition of ethylene glycol at low temperature, J. Porous. Mater. 24 (2017) 779–786, https://doi.org/10.1007/s10934-016-0316-7.
[51] K. Nielsch, J. Choi, K. Schwirn, R.B. Wehrspohn, U. Gösele, Self-ordering regimes of porous alumina: the 10 porosity rule, Nano Lett. 2 (2002) 677–680, https://doi.org/10.1021/nl025537k.
[52] A.L. Friedman, D. Brittain, L. Menon, Roles of pH and acid type in the anodic growth of porous alumina, J. Chem. Phys. 127 (2007), https://doi.org/10.1063/1.2790429.